

Analysis and Prediction of Influencing Parameters on the Coal Classification Performance of a Novel Three Products Hydrocyclone Screen (TPHS) Based on Grey System Theory

Authors:

Chuanzhen Wang, Xiaolu Sun, Liang Shen, Guanghui Wang

Date Submitted: 2020-12-22

Keywords: GM(1, N) model, Grey System theory, performance prediction, three products hydrocyclone screen, performance analysis

Abstract:

A novel hydrocyclone including a cylindrical screen embedded in a conventional hydrocyclone (CH), named three products hydrocyclone screen (TPHS), has been successfully designed. In TPHS, the combination of centrifugal classification and screening was employed to separate particles. In this paper, Grey theory, as an effective means to the laws of both complex and uncertainty system's behavior with small samples, was used to investigate the operational (feed concentration and feed pressure) and structural (aperture size, spigot diameter, and vortex finder diameter) parameters on performance evaluation Hancock classification efficiency (HE), imperfection (I), and cut size (d50c). The experiments of coal sample (0?1 mm) show that TPHS with coarser particles in underflow exhibited the absent "fish-hook". The closeness calculated using the Grey System algorithm indicates that the performance of TPHS was closely related to the operation and structure parameters. Further, the order of grey incidence degree between different parameters and HE (or I or d50c) is the spigot diameter and aperture size with the highest value, the feed pressure and vortex finder diameter with the middle value, and the feed concentration with the lowest value. The prediction using the GM(1, N) algorithm implies that the dynamic prediction model for the performance evaluation can be created depending on the operation, structure and previous performance value. The mean relative errors between the predicted and actual HE, I, and d50 were 2.84%, 5.83%, and 3.57%, respectively, which exhibit the accurate prediction.

Record Type: Published Article

Submitted To: LAPSE (Living Archive for Process Systems Engineering)

Citation (overall record, always the latest version):

LAPSE:2020.1249

Citation (this specific file, latest version):

LAPSE:2020.1249-1

Citation (this specific file, this version):



LAPSE:2020.1249-1v1

DOI of Published Version: <https://doi.org/10.3390/pr8080974>

License: Creative Commons Attribution 4.0 International (CC BY 4.0)

Article

Analysis and Prediction of Influencing Parameters on the Coal Classification Performance of a Novel Three Products Hydrocyclone Screen (TPHS) Based on Grey System Theory

Chuanzhen Wang ^{1,†} , Xiaolu Sun ^{2,*,†}, Liang Shen ^{1,*}  and Guanghui Wang ³

¹ State Key Laboratory of Mining Response and Disaster Prevention and Control in Deep Coal Mines, College of Material Science and Engineering, Anhui University of Science and Technology, Huainan 232001, China; faxofking@cumt.edu.cn

² School of Mining and Technology, Inner Mongolia University of Technology, Hohhot 010051, China

³ Key Laboratory of Coal Processing and Efficient Utilization, Ministry of Education, School of Chemical Engineering and Technology, China University of Mining & Technology, Xuzhou 221116, China; wgh1015@163.com

* Correspondence: sunxl@imut.edu.cn (X.S.); shen654520@aust.edu.cn (L.S.); Tel.: +86-188-5214-6286 (X.S.); +86-187-5698-9875 (L.S.)

† C.W. and X.S. contributed equally.

Received: 16 June 2020; Accepted: 6 August 2020; Published: 12 August 2020



Abstract: A novel hydrocyclone including a cylindrical screen embedded in a conventional hydrocyclone (CH), named three products hydrocyclone screen (TPHS), has been successfully designed. In TPHS, the combination of centrifugal classification and screening was employed to separate particles. In this paper, Grey theory, as an effective means to the laws of both complex and uncertainty system's behavior with small samples, was used to investigate the operational (feed concentration and feed pressure) and structural (aperture size, spigot diameter, and vortex finder diameter) parameters on performance evaluation Hancock classification efficiency (HE), imperfection (I), and cut size (d_{50c}). The experiments of coal sample (0–1 mm) show that TPHS with coarser particles in underflow exhibited the absent “fish-hook”. The closeness calculated using the Grey System algorithm indicates that the performance of TPHS was closely related to the operation and structure parameters. Further, the order of grey incidence degree between different parameters and HE (or I or d_{50c}) is the spigot diameter and aperture size with the highest value, the feed pressure and vortex finder diameter with the middle value, and the feed concentration with the lowest value. The prediction using the GM(1, N) algorithm implies that the dynamic prediction model for the performance evaluation can be created depending on the operation, structure and previous performance value. The mean relative errors between the predicted and actual HE , I , and d_{50} were 2.84%, 5.83%, and 3.57%, respectively, which exhibit the accurate prediction.

Keywords: three products hydrocyclone screen; performance analysis; performance prediction; Grey System theory; GM(1, N) model

1. Introduction

Hydrocyclones are well known as significant devices to separate fine particles based on its size in a centrifugal force field. According to the high throughput, low cost, flexible operation and so on, hydrocyclones are now widely used in mineral, chemical, environmental, and some other industrial processes [1–3]. The conventional hydrocyclone (CH) includes one tangential feed inlet and two axial

product outlets, i.e., smaller underflow at the bottom and bigger overflow at the top to discharge coarser and fine particles, respectively [4,5]. Nevertheless, on the one hand due to the inherent disadvantages (like fish-hook effect or unsatisfactory efficiency [6,7]), on the other hand owing to the new trends (like the reducing processed particle size [8,9]), the hydrocyclone performance is partly weak, even the device cannot be adopted in some industrial process cases. Therefore, the device performance is tried to be improved by the structural modifications, such as (1) introducing new structures like filtering hydrocyclone [10,11], JK three-product cyclone [12], and two-inlet hydrocyclones [13,14], and (2) changing original structures including the feed pipe [15], the cylindrical section [16], the vortex finder [17], and the conical vessel [16], among others.

In view of the above-mentioned types of hydrocyclone, a new apparatus called three products hydrocyclone screen (TPHS) shown in Figure 1 has been developed [18,19]. Basically, TPHS can be considered as a CH embedded by a cylindrical screen to combine both centrifugal classification and screening. Thus, cylinder stratification, cylinder classification, and cone classification are generated in TPHS to separate particle depending on size. The working process between TPHS and CH are similar; however, besides the overflow and underflow, the present screen results in a new screen underflow product in TPHS. The previous experiment for TPHS and CH expose that the new cyclone could remove the “fish-hook” effect for better performances [18]. In addition, the exited computational fluid dynamics simulation and particle image velocimetry test reveal that TPHS, compared to CH, could eliminate the air column and short circuit flow for the more reasonable flow field distribution [20].

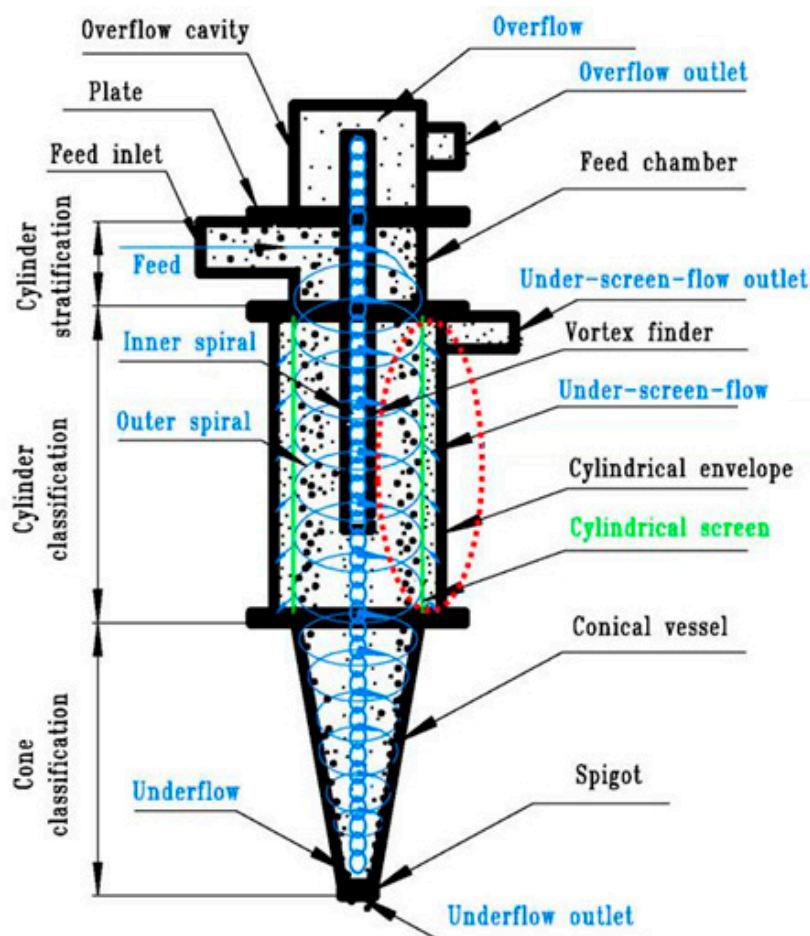


Figure 1. Schematic diagram of the three-product hydro-cyclone (TPHS) [18].

The previous researches demonstrate that some general understanding for TPHS is available. However, the previous research focused on the performance contrast of TPHS and CH; the details

of effects of structural and operational parameters on TPHS are not yet reported and remains unexplored. To cyclone, Hancock classification efficiency, imperfection, and cut size are the important indexes to generally evaluate the device performance of cyclone, which are closely related to both operation parameters (including feed concentration and feed pressure) and structure parameters (cyclone diameter, vortex finder diameter, and spigot diameter) [21]. Since, TPHS is a derivative of hydrocyclones, the aforesaid parameters can be considered for the performance evaluation of the new cyclone. However, due to the particular cylindrical screen, the aperture size should be taken as one vital factor for TPHS performance. Usually, the experiments under different factors are adopted to explore the influence of conditions on cyclone performance [4], wherein the experiment result should be analyzed through the suitable data processing method.

Recently, with the development of data processing algorithm, Grey System theory [22–24] has been considered as an effective means to the laws of both complex and uncertainty systems' behavior with small samples. As this algorithm explores the objective laws through information coverage and through the works of sequence operators, it is little constrained by experimental conditions. Thus, Grey System theory has been widely used in many fields including hydrocyclone [25–27]. Therefore, this method can be as well applied to the performance of TPHS.

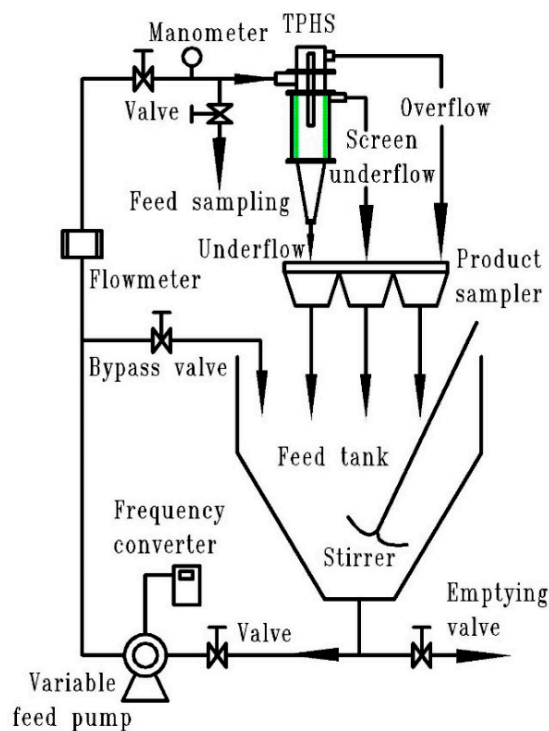
Thus, based on the above discussion, the objective of this new investigation was to explore the device performance involving different operational and structural parameters for the aforementioned knowledge gap. To attain this purpose, Grey System theory has been used, considering a pilot-scale TPHS (φ 150 mm). Specifically, the objectives of the present study were to:

- (1) Comprehensively verify the separation characteristic including the size distribution and the partition curve;
- (2) systematically explore the closeness between the performance and the relevant factors (operational and structural); and
- (3) critically analyze and verify the prediction model of the performance evaluation based on the parameters of operation and structure.

2. Experimental

2.1. Experiment Rig

The diagram of experiment rig is exhibited in Figure 2a schematic diagram and (b) photograph. From this figure, it can be seen that the main devices adopted in the present study included a feed tank of 0.5 m³, a variable feed pump of 0–30 m³/h, a frequency converter of 0–50 Hz, a product sampler, some valves, a stirrer and a TPHS. An electromagnetic flow meter and a mechanical manometer were used to measure the feed mass flow and pressure, respectively. It is worth pointing out that the TPHS size and the target cut size were considered as 150 mm and 0.25 mm, respectively in terms of our previous work [18]. The details of structure parameters for TPHS are shown in Table 1. The aperture size of the cylindrical screen was in the range of ~0.5 mm to 0.7 mm (~2 to 3 times bigger than the target cut size). The length of inlet column and cylindrical envelope were 130 mm and 370 mm, respectively. The length of vortex finder was 300–400 mm. The size of inlet was 58 mm × 26 mm for feed stream. The spigot diameter of 18 mm and 24 mm and the cone angle of 20° were used to generate the crowding and hindered settling conditions in the cone classification for underflow stream. The diameter of vortex finder was considered ~30 mm to 60 mm for overflow stream.



(a) schematic diagram



(b) photograph

Figure 2. Pilot-scale experiment rig for TPHS.**Table 1.** Structures of TPHS in pilot-scale experiment.

Items	Value
Diameter of hydrocyclone	150 mm
Aperture size of cylindrical screen	0.5 mm, 0.6 mm and 0.7 mm
Length of inlet column	130 mm
Length of cylindrical envelope	370 mm
Length of vortex finder	300–400 mm
Angle of cone	20°
Size of inlet	58 mm × 16 mm
Diameter of screen underflow outlet	56 mm
Diameter of vortex finder	30 mm, 40 mm, 50 mm, 60 mm
Diameter of spigot	18 mm, 24 mm

2.2. Experiment Procedure

In this research, the coal samples (diameter $\sim 0\text{--}1$ mm and density ~ 1.45 g/cm³) from Guobei coal preparation plant, China, were used as the mineral particles. The experiment procedure can be described as follows.

- (1) The process cycle starts with a coal slurry being stirred ~ 10 min. Subsequently the homogeneous slurry was reported to TPHS by the variable speed pump with different experiment conditions (see Table 2 for the details). Based on the previous works [18,19], the operational parameters feed concentration and feed pressure were considered as 60–220 g/L and 0.04–0.06 MPa, respectively, while the structural parameters aperture size, spigot diameter and vortex finder diameter were 0.60–0.80 mm, 18.00–24.00 mm, and 30.00–60.00 mm, respectively. As mentioned, Grey System theory is less limited to the experimental conditions., thus different parameters were combined from large to small in the present research.

Table 2. Experimental conditions.

Experiment Number	1	2	3	4	5	6	7	8	9	10
Feed concentration (g/L)	60.00	100.00	140.00	180.00	220.00	60.00	100.00	140.00	180.00	220.00
Feed pressure (MPa)	0.04	0.05	0.06	0.04	0.05	0.06	0.04	0.05	0.06	0.04
Aperture size (mm)	0.60	0.70	0.80	0.60	0.70	0.80	0.60	0.70	0.80	0.60
Diameter of spigot (mm)	18.00	24.00	18.00	24.00	18.00	24.00	18.00	24.00	18.00	24.00
Diameter of vortex finder (mm)	30.00	40.00	50.00	60.00	30.00	40.00	50.00	60.00	30.00	40.00

- (2) Then, every experiment was run about 30 min to get the steady particle separation. Afterwards, the inlet and outlet streams were sampled simultaneously, where three sets of each stream sample were taken with the intervals of 5 min, i.e., at 40, 45, and 50 min for the sample representativeness.
- (3) Finally, all the samples were processed by the weighing, filtration, and drying for the granularity test. It is noted that wet sieving [28] was considered for the analysis of particle size distribution to avoid the particle aggregation.

2.3. Data Analysis

In this research, the mass flow ratio of solids, i.e., solid recovery, for each product stream was calculated by Equations (1)–(4) according to the least-squares method (LSM) [29]. So as to eliminate the effect of the bypass to underflow [30,31], the corrected partition curve was conducted using Equations (5) and (6). To evaluate the performance of TPHS, Hancock classification efficiency (HE) and the imperfection (I) was obtained by Equations (7) and (8), respectively [32–34], and the corrected cut size of the partition curve (d_{50c}) was gotten according to its definition (see the details in the annotation after Equation (8)). The Equations (1)–(8) are shown as follows:

$$\gamma_1 = \frac{g_{01}g_{22} - g_{02}g_{12}}{g_{11}g_{22} - g_{12}g_{21}} g \times 100\% \quad (1)$$

$$\gamma_2 = \frac{g_{02}g_{11} - g_{01}g_{12}}{g_{11}g_{22} - g_{12}g_{21}} g \times 100\% \quad (2)$$

$$\gamma_3 = 100\% - \gamma_1 - \gamma_2 \quad (3)$$

$$\left. \begin{aligned} g_{01} &= \sum_{j=1}^N (G_{0j} - G_{3j})(G_{1j} - G_{3j}) \\ g_{11} &= \sum_{j=1}^N (G_{0j} - G_{3j})^2 \\ g_{02} &= \sum_{j=1}^N (G_{0j} - G_{3j})(G_{2j} - G_{3j}) \\ g_{12} &= \sum_{j=1}^N (G_{1j} - G_{3j})(G_{2j} - G_{3j}) \\ g_{22} &= \sum_{j=1}^N (G_{2j} - G_{3j})^2 \end{aligned} \right\} \quad (4)$$

$$P_{tj} = \frac{\gamma_3 G_{3j}}{G_{0j}} \quad (5)$$

$$P_{cj} = \frac{P_{tj} - R_f}{100\% - R_f} \quad (6)$$

$$HE = \left[\frac{\gamma_3 \times (-d_{t3})}{-d_{t0}} + \frac{\gamma_3 \times (+d_{t3})}{+d_{t0}} \right] - 100\% \quad (7)$$

$$I = \frac{d_{75c} - d_{25c}}{2d_{50c}} \quad (8)$$

where, γ_1, γ_2 , and γ_3 represent the solid recovery in the overflow, screen underflow and underflow, respectively. G_{0j}, G_{1j}, G_{2j} , and G_{3j} are the mass percentage of the particle size interval (j) in the feed, overflow, screen underflow and underflow, respectively. P_{tj} means the partition number of the raw partition curve for the particle size interval (j). P_{cj} means the partition number of the corrected partition curve for the particle size interval (j), R_j indicates the percentage of water from the feed to the underflow. $+d_{t3}$ and $-d_{t3}$ is the cumulative weight percentage in underflow which size is coarser and finer than the target cut size, respectively. $+d_{t0}$ and $-d_{t0}$ are the cumulative weight percentage in the feed which size is coarser and finer than the target cut size, respectively. d_{25c}, d_{50c} , and d_{75c} are the particle size corresponding to the partition numbers 25%, 50%, and 75% from the corrected partition curve, respectively. d_{50c} is usually named corrected cut size of the partition curve.

In the present study, the grey system theory was used to explore the action law of different operational and structural factors on TPHS. Wherein, the grey system algorithm, given in Equations (9) and (10), was assumed to analyze the closeness between the performance and different operational and structural parameters, while the GM(1, N) algorithm [23,24] in Equations (11)–(14) was used to predict the performance evaluation for TPHS. The Equations (9)–(14) are shown as follows:

$$r(\overline{X_0}, \overline{X_l}) = \frac{1}{n} \sum_{k=1}^n r(\overline{x_0}(k), \overline{x_l}(k)) \tag{9}$$

$$\left. \begin{aligned} \overline{X_0} &= (x_0(1), x_0(2), \dots, x_0(m))x_0(1)^{-1} = \left(\frac{x_0(1)}{x_0(1)}, \frac{x_0(2)}{x_0(1)}, \dots, \frac{x_0(m)}{x_0(1)}\right)x_0(1) \neq 0 \\ \overline{X_l} &= (x_l(1), x_l(2), \dots, x_l(n))x_l(1)^{-1} = \left(\frac{x_l(1)}{x_l(1)}, \frac{x_l(2)}{x_l(1)}, \dots, \frac{x_l(n)}{x_l(1)}\right)x_l(1) \neq 0 \text{ and } l = 1, 2, \dots, n \\ r(\overline{x_0}(k), \overline{x_l}(k)) &= \frac{\min_k \min_l |\overline{x_0}(k) - \overline{x_l}(k)| + \xi \max_k \max_l |\overline{x_0}(k) - \overline{x_l}(k)|}{|\overline{x_0}(k) - \overline{x_l}(k)| + \xi \max_k \max_l |\overline{x_0}(k) - \overline{x_l}(k)|} \quad k = 1, 2, \dots, m \end{aligned} \right\} \tag{10}$$

$$\overline{x_0}(k) = az_0^{(1)}(k) + \sum_{l=1}^n b_l \overline{x_l}^{(1)}(k) \tag{11}$$

$$\left. \begin{aligned} \overline{x_l}^{(1)}(k) &= \sum \overline{x_l}(k) \quad k = 1, 2, \dots, m \\ \overline{x_0}^{(1)}(k) &= \sum \overline{x_0}(k) \quad k = 1, 2, \dots, m \\ z_0^{(1)}(k) &= \frac{\overline{x_0}^{(1)}(k) + \overline{x_0}^{(1)}(k-1)}{2} \quad k = 2, \dots, m \end{aligned} \right\} \tag{12}$$

$$\hat{a} = [a, b_1, b_2, \dots, b_n] = (\mathbf{B}^T \mathbf{B})^{-1} \mathbf{B}^T \mathbf{y} \tag{13}$$

$$\mathbf{B} = \begin{bmatrix} z_0^{(1)}(2) \overline{x_1}^{(1)}(2) \dots \overline{x_n}^{(1)}(2) \\ \dots \dots \dots \\ z_0^{(1)}(m) \overline{x_1}^{(1)}(m) \dots \overline{x_n}^{(1)}(m) \end{bmatrix}, \mathbf{y} = \begin{bmatrix} \overline{x_1}^{(1)}(2) \\ \vdots \\ \overline{x_1}^{(1)}(m) \end{bmatrix} \tag{14}$$

where, X_0 and X_l stand the actual performance sequence (i.e., HE, etc.) and relevant factor sequence (i.e., feed concentration, etc.) of the system, respectively. $\overline{X_0}$ and $\overline{X_l}$ are the dimensionless values of X_0 and X_l , respectively. $\overline{x_0}(k)$ and $\overline{x_l}(k)$ are referred to as the value of the sequence $\overline{X_0}$ and $\overline{X_l}$, respectively, at point k . $r(\overline{X_0}, \overline{X_l})$ represents the relative degree of grey incidence between $\overline{X_0}$ and $\overline{X_l}$ at point k . $\xi \in (0, 1)$ means the distinguishing coefficient (equaled 0.5 in this study). The subscript l represents the l row in sequence. m and n are the number of the experiment and system's relevant factor, respectively. the constant a related to the performance evaluation is known as the development coefficient of the system. $b_l \overline{x_l}^{(1)}(k)$ and b_l are the driving term and driving coefficient, respectively, which are related to the relevant factor of system. $\overline{x_0}^{(1)}(k)$ and $\overline{x_l}^{(1)}(k)$ are the accumulated generation operation (AGO) of $\overline{x_0}(k)$ and $\overline{x_l}(k)$, respectively. $z_0^{(1)}(k)$ is the mean generation of $\overline{x_0}(k)$.

3. Results and Discussions

Prior to the investigation for the effects of operational and structural parameters on the device performance, the separation characteristic of TPHS was verified compared to previous works. Following this, the closeness between the performance and the relevant factors (operation and structure parameters) was systematically explored using the Grey System theory. Then, the prediction and verification for the performance evaluation of TPHS were obtained by the GM(1, N) model. The details are described as follows.

3.1. Separation Characteristic

Figure 3a–c describes the particle size distribution for (a) overflow (b) screen underflow and (c) underflow in the TPHS at different experiments (experiment factors shown in Table 2). The particle size distribution for feed corresponding to each experiment is shown in Figure A1 in the Appendix C. It is apparent that the size distribution of TPHS in each product stream varied with different operational and structural parameters, however, the overall trends remained similar. In general, the size distribution in overflow and screen underflow were finer than that in underflow. Particularly, the dominant size distribution in screen underflow was in the range of ~0 mm to 0.25 mm, which was similar to that in overflow (~0 to 0.25 mm), relative to that in underflow (0.25 to 1 mm). It can be attributed to the adding cylindrical screen which combined centrifugal separation and screening [18].

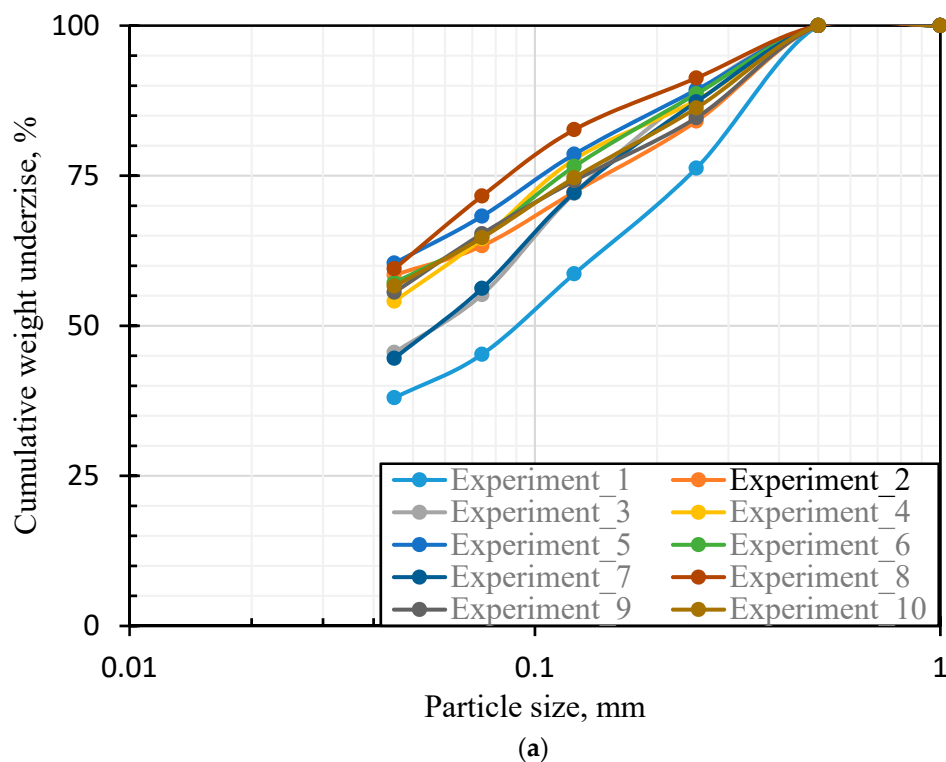


Figure 3. Cont.

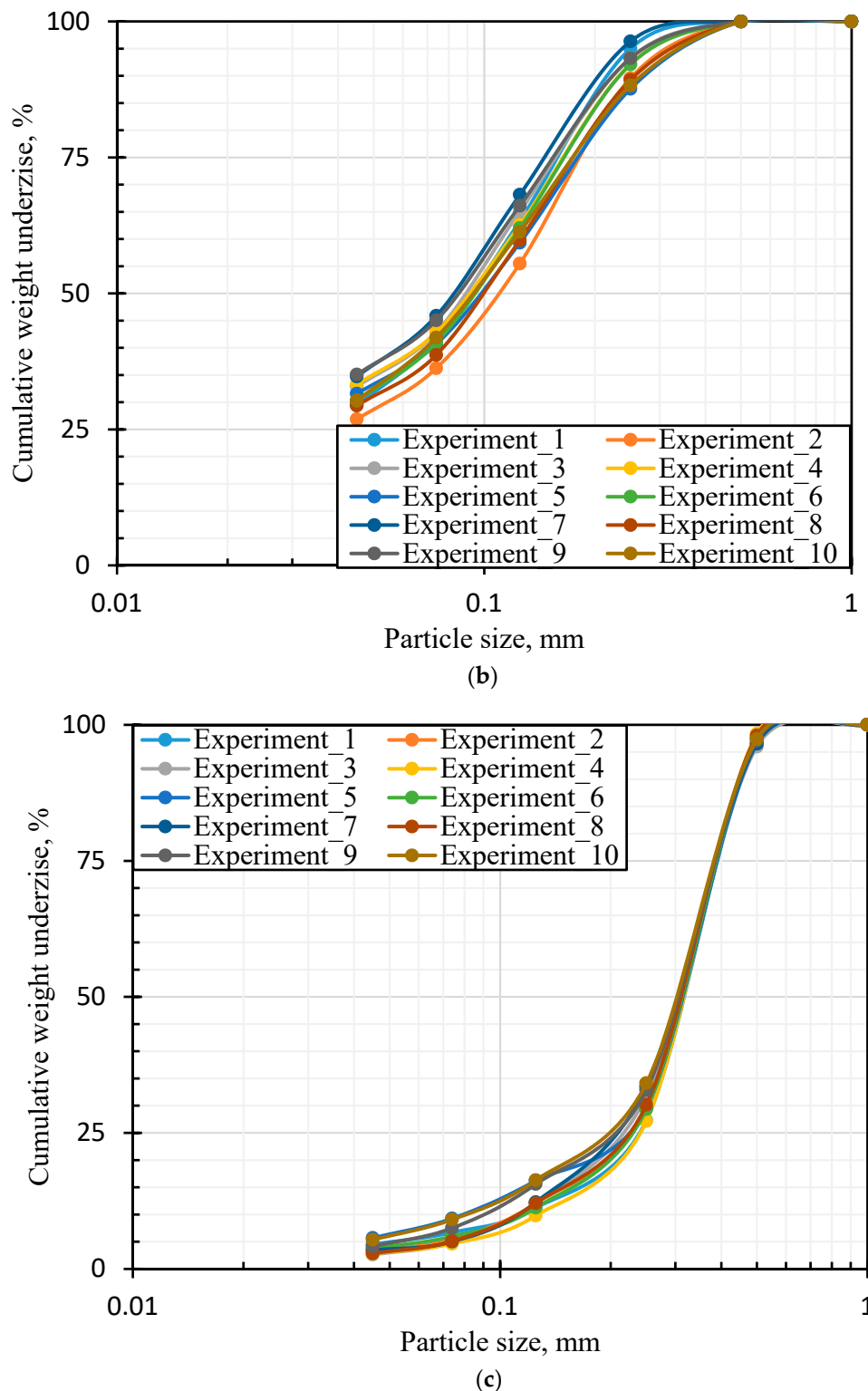


Figure 3. Size distribution for TPHS (a) overflow, (b) screen underflow, and (c) underflow.

The solid recovery and water recovery of each product stream for TPHS are exhibited in Table 3, which were estimated using the formulas above (Equations (1)–(4)) and the definition, respectively. It is evident that the solid recovery in both underflow and screen underflow was more than that in overflow, which demonstrates that fewer particles discharged via overflow. In addition, the water recovery in underflow was less than that in overflow and screen underflow, which indicates that less water (i.e., lower bypass flow fraction [31]) flowed through underflow stream. In Figure 4, the absent

“fish-hook” can be observed distinctly in all corrected partition curves (plotted by Equations (5) and (6)) of TPHS, which leads to the fewer fines sent to underflow and the increasing device performance. This result can be ascribed to the presence of cylindrical screen that altered the size distribution in each product stream [18]. Both the above size distribution and the corrected partition curves of TPHS shows the similar trends to the literature [18], which also verifies the reasonable results in this work.

Table 3. Solid recovery of each product stream and water recovery of underflow.

Experiment Number	Solid Recovery in Overflow γ_1 (%)	Solid Recovery in Screen Underflow γ_2 (%)	Solid Recovery in Underflow γ_3 (%)	Water Recovery in Underflow R_f (%)
1	12.76	32.20	55.04	10.26
2	13.20	40.30	46.48	6.87
3	17.77	39.04	43.19	4.89
4	9.43	46.85	43.72	5.39
5	13.05	51.38	35.57	7.41
6	5.69	42.74	51.57	6.01
7	27.30	34.45	38.28	3.35
8	12.49	47.91	39.60	3.95
9	6.45	52.79	40.76	6.62
10	10.40	52.54	37.07	8.16

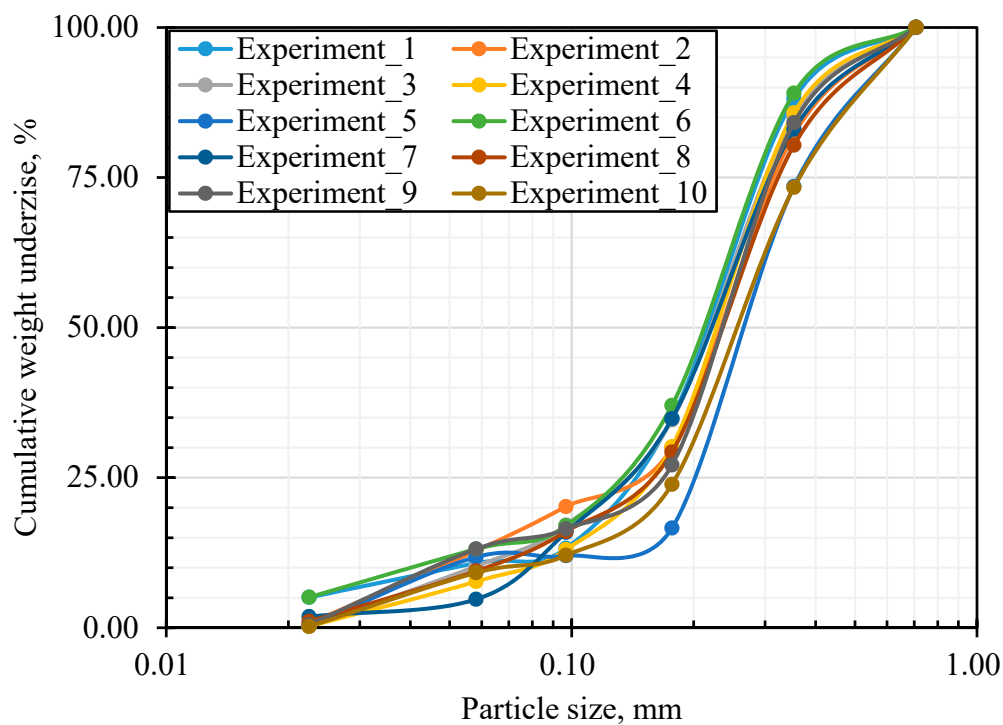


Figure 4. Corrected partition curves of TPHS.

3.2. Closeness Analysis

Table 4 shows the performance evaluation (HE , I , and d_{50c}) under different operation and structure factors (feed concentration, feed pressure, aperture size, spigot diameter, and vortex finder diameter) for TPHS in the present study. The HE and I were calculated using Equations (7) and (8), respectively, while d_{50c} was estimated according to its definition. It is distinct that the performance evaluation HE , I and d_{50c} of TPHS fluctuates around 63%, 0.363 and 0.248 mm, respectively, with different factors.

Table 4. Performance evaluation under different relevant factors for TPHS.

Items			Experiment Number									
			1	2	3	4	5	6	7	8	9	10
Performance X_0	X_0	<i>HE</i> (%)	61.160	60.854	63.515	67.908	57.911	63.948	64.665	65.155	64.626	59.310
	X_0	<i>I</i>	0.370	0.380	0.383	0.347	0.307	0.380	0.396	0.360	0.340	0.365
	X_0	d_{50c} (mm)	0.230	0.250	0.235	0.245	0.285	0.230	0.240	0.250	0.250	0.260
Relevant factors X_1	X_1	Feed concentration (g/L)	60.00	100.00	140.00	180.00	220.00	60.00	100.00	140.00	180.00	220.00
	X_2	Feed pressure (MPa)	0.04	0.05	0.06	0.04	0.05	0.06	0.04	0.05	0.06	0.04
	X_3	Aperture size (mm)	0.60	0.70	0.80	0.60	0.70	0.80	0.60	0.70	0.80	0.60
	X_4	Diameter of spigot (mm)	18.00	24.00	18.00	24.00	18.00	24.00	18.00	24.00	18.00	24.00
	X_5	Diameter of vortex finder (mm)	30.00	40.00	50.00	60.00	30.00	40.00	50.00	60.00	30.00	40.00

To explore the effect of the operation and structure parameters on the performance of TPHS, the relative degree of grey incidence was obtained using Equations (9) and (10), which is shown in Figure 5. It is noted that the relative degree of grey incidence can be considered to reflect the closeness of the relationship between parameters and performance evaluation. The bigger relative degree of grey incidence reveals the higher closeness, vice versa. The details for the calculation are shown in Appendix A. From Figure 5, it is found that both the operational and structural parameters mainly influenced the device performance, in which the relative grey incidence degree of each factor was more than 0.5. In detail, the diameter of spigot shows the highest grey incidence degree of 0.895 and 0.878 for the HE and I , respectively, while the aperture size presents the highest grey incidence degree of 0.895 for the d_{50c} . Further, the feed pressure and vortex finder diameter display the smaller grey incidence degree which were $\sim 97\%$ and $\sim 88\%$ of the highest degree, respectively. Besides, the feed concentration exhibits the smallest grey incidence degree to each performance evaluation, which was only $\sim 65\%$ of the highest degree. Thus, the order of the grey incidence degree for the performance of TPHS can be summarized as follows: Spigot diameter and aperture size the highest, followed by feed pressure and vortex finder diameter, feed concentration the lowest. This trend reveals that the structure consisting of the spigot diameter and aperture size plays significant roles in the device performance, compared to the operation including feed pressure and feed concentration. To a certain extent, this trait also indicates that TPHS shows good adaptability to the operation conditions.

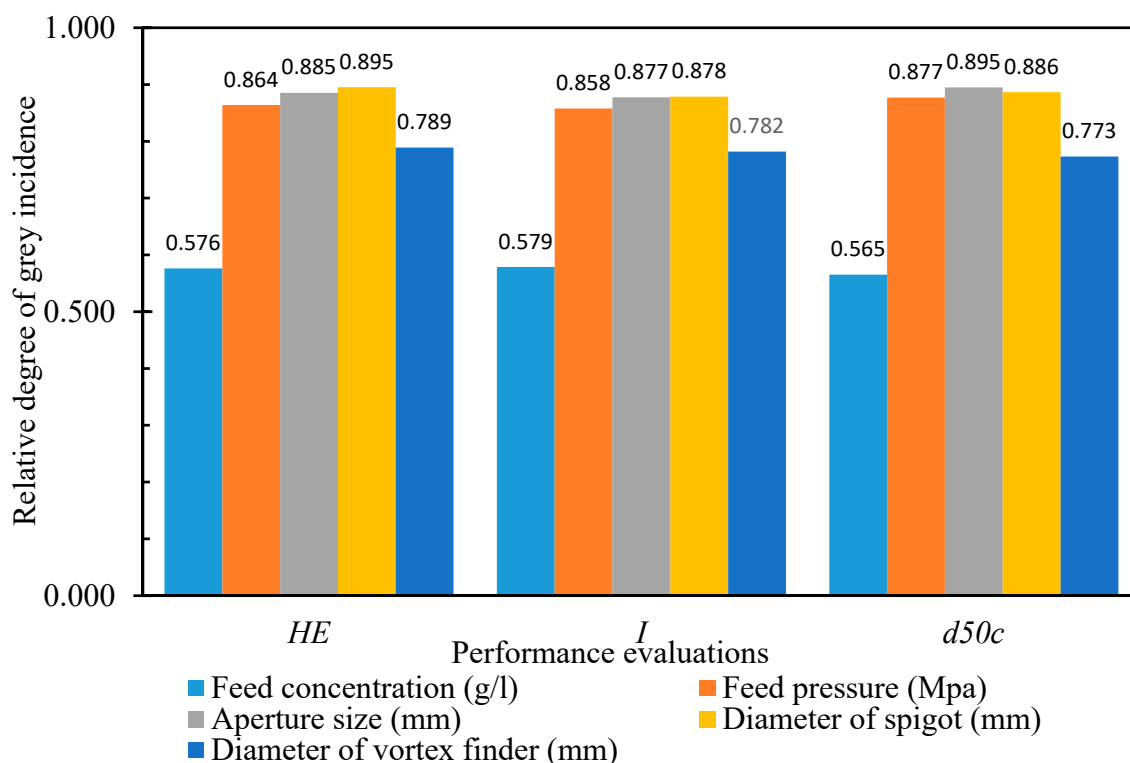


Figure 5. Relative degree of grey incidence for the performance in TPHS.

3.3. Prediction and Verification

To predict the performance of TPHS, the dimensionless sequence \overline{X}_0 and \overline{X}_l (see Table A1 in Appendix A) were conducted using the aforesaid GM(1, N) model (see Appendix B for the details of calculation). The sequence of parameter \hat{a} given by Equations (13) and (14) are described in Table 5, while the prediction models were obtained using Equations (11) and (12) for the dimensionless value of HE , I and d_{50c} are shown in Equation (15). Note that the coefficient a , b_1 , b_2 , b_3 , b_4 , and b_5 in Equation

(13) were corresponding to the *HE* (or *I* or d_{50c}), feed concentration, feed pressure, aperture size, spigot size, and vortex finder diameter, respectively.

Table 5. Parameter \hat{a} for the dimensionless performance evaluation in TPHS.

Items	Parameter \hat{a}	<i>HE</i> (%)	<i>I</i>	d_{50c} (mm)
Development coefficient of system	<i>a</i>	−1.842	−1.604	−1.690
Driving coefficient b_1	b_1	−0.019	−0.129	0.065
	b_2	−6.227	−9.021	−9.541
	b_3	7.902	10.994	11.632
	b_4	−0.001	0.016	−0.127
	b_5	0.175	−0.035	−0.142

From Table 5, it is apparent that the systematic development coefficient *a* was negative to the prediction of *HE*, *I* and d_{50c} , while the driving coefficient $b_1 \sim b_5$ fluctuated with different performance evaluations. In detail, the $b_1 \sim b_2$ and b_3 were negative and positive, respectively, to all the prediction value. The b_4 was negative and positive to the predicted *HE* (or d_{50c}) and *I*, respectively, while the b_5 was negative and positive to the predicted *I* (or d_{50c}) and *HE*, respectively. The present prediction model indicates that the predicted dimensionless *HE* (*I* or d_{50c}) reduced with the decreasing accumulated generation operation (AGO) of the aperture size or the increasing AGO of the previous *HE* (*I* or d_{50c}), feed concentration and feed pressure. Further, with the increasing AGO of the spigot size, the predicted *HE* and d_{50c} decreased but the predicted *I* increased. Conversely, as the AGO of the vortex finder diameter rose, the predicted *HE* went up yet the *I* and d_{50c} went down. Note that the systematic development coefficient *a* related to the AGO of the *HE* (*I* or d_{50c}) was used in the GM(1, N) model. Thus, the prediction model (Equation (15)) for the performance evaluation of TPHS can be dynamically updated according to the actual operation, which improves the applicability and accuracy of the prediction model.

$$\begin{bmatrix} \bar{x}_0(k)_{HE} \\ \bar{x}_0(k)_I \\ \bar{x}_0(k)_{d_{50c}} \end{bmatrix} = \begin{bmatrix} -0.959 & -0.010 & -3.242 & 4.113 & -0.0004 & 0.091 \\ -1.604 & -0.129 & -9.021 & 10.994 & 0.016 & -0.035 \\ -0.916 & -0.035 & -6.171 & 6.305 & -0.0687 & -0.077 \end{bmatrix} \begin{bmatrix} \bar{x}_0^{(1)}(k-1)_{HE} & \bar{x}_0^{(1)}(k-1)_I & \bar{x}_0^{(1)}(k-1)_{d_{50c}} \\ \bar{x}_1^{(1)}(k) & \bar{x}_1^{(1)}(k) & \bar{x}_1^{(1)}(k) \\ \bar{x}_2^{(1)}(k) & \bar{x}_2^{(1)}(k) & \bar{x}_2^{(1)}(k) \\ \bar{x}_3^{(1)}(k) & \bar{x}_3^{(1)}(k) & \bar{x}_3^{(1)}(k) \\ \bar{x}_4^{(1)}(k) & \bar{x}_4^{(1)}(k) & \bar{x}_4^{(1)}(k) \\ \bar{x}_5^{(1)}(k) & \bar{x}_5^{(1)}(k) & \bar{x}_5^{(1)}(k) \end{bmatrix} \quad (15)$$

The comparison between the predicted and actual value for *HE*, *I* and d_{50c} under the above experiment 1–10 (see Table 2 for experiment details) was used to verify the accuracy of prediction model. From the dimensionless performance evaluation (Equation (10)) for TPHS, the predicted dimensionless values which times the corresponding $x_0(1)$ can be converted to the prediction of *HE*, *I*, and d_{50c} , respectively. Figure 6 shows the comparison of the actual and predicted performance evaluation (a) *HE* (b) *I* and (c) d_{50c} , while the relative error and mean relative error are presented in Table 6. In Figure 6, it is evident that the performance predicted by the Equations (14)–(16) shows good agreement with that obtained by the actual experiment (from experiment 1–10). From Table 6, it can be seen that although the relative error fluctuated, the mean relative error between the actual and predicted *HE*, *I*, and d_{50c} were 2.84%, 5.83%, and 3.57%, respectively. This result demonstrates that the prediction models obtained using the GM(1, N) model can well predict the performance evaluation *HE*, *I*, and d_{50c} for TPHS.

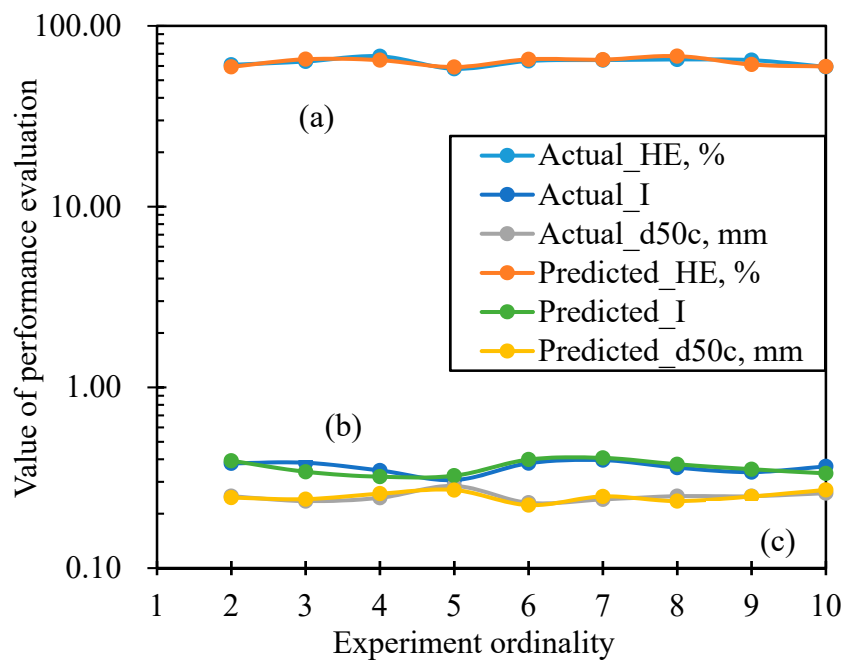


Figure 6. Comparison of the actual and predicted performance evaluation (a) Hancock classification efficiency HE (b) imperfection I and (c) cut size of corrected partition curve d_{50c} for TPHS.

Table 6. Error checks.

Items	Relative Error = (Predicted-Actual)/Predicted*100%			
	HE	I	d_{50c}	
Experiment	2	-2.49%	3.35%	-1.76%
	3	2.93%	-10.86%	2.50%
	4	-4.88%	-7.58%	5.42%
	5	2.22%	5.71%	-5.09%
	6	2.11%	4.81%	-2.96%
	7	0.62%	2.91%	3.86%
	8	4.44%	4.36%	-6.00%
	9	-5.44%	3.64%	-0.27%
	10	0.37%	-8.52%	4.26%
	Mean relative error, %	2.83%	5.75%	3.57%

4. Conclusions

In the present study, a new three products hydrocyclone screen (TPHS) which combine both centrifugal classification and screening to separate particle depending on size has been successfully developed. The pilot-scale experiments of coal samples (0–1 mm) were widely carried out conducting a 150-mm TPHS aiming to explore the effects of operation (feed concentration and feed pressure) and structure (aperture size, spigot diameter, and vortex finder diameter) parameters on the device performance (Hancock classification efficiency (HE), imperfection (I), and the cut size (d_{50c}). The obtained results were verified firstly, and then critically analyzed using the Grey System algorithm and GM(1, N) algorithm. Based on the presented results, the following conclusions can be obtained:

- (1) In TPHS, the size distribution in overflow and screen underflow was finer than that in underflow, further, the absent “fish-hook” can be observed due to the presence of cylindrical screen. This is consistent with the previous literature.
- (2) The closeness analysis using the Grey System theory reveals that the operational and structural parameters greatly influenced the performance of TPHS with the relative grey incidence degree

of ~0.5 to 1. Further, the order of grey incidence degree between different parameters and *HE* (or *I* or d_{50c}) is that: The spigot diameter and aperture size present the highest incidence degree; the feed pressure and vortex finder diameter exhibit the middle incidence degree; and the feed concentration shows the lowest incidence degree.

- (3) The dynamic performance prediction model using the GM(1, N) can be generated according to the operation, structure, and previous performance value. As the accumulated generation operation (AGO) of the aperture size decreased or the AGO of the previous *HE* (*I* or d_{50c}), feed concentration and feed pressure increased, the predicted *HE* (*I* or d_{50c}) decreased. Besides, the predicted *HE* and d_{50c} reduced but the predicted *I* improved with the increasing AGO of the spigot size, while the predicted *HE* declined yet the *I* and d_{50c} increased with the growing AGO of the vortex finder diameter.
- (4) The performance evaluations estimated using the prediction model present excellent agreement with those gotten using the actual pilot-scale experiment, wherein the mean relative errors were 2.84%, 5.83%, and 3.57%, respectively.

Author Contributions: C.W. and X.S. equally contributed of conceptualization, formal analysis, investigation, methodology, writing—original draft and writing—review & editing; L.S. contributed of software, supervision, validation and visualization; G.W. contributed of funding acquisition, project administration and resources. All authors have read and agreed to the published version of the manuscript.

Funding: This research was funded by Anhui Provincial Natural Science Foundation grant number 2008085QE272; China Postdoctoral Science Foundation grant number 2020M671837; Key Research and Development Plan Projects in Anhui Province grant number 202004a07020044; Research Program of science and technology at Universities of Inner Mongolia Autonomous Region grant number NJZY20083; Doctor foundation of Anhui University of science and technology; University-level key projects of Anhui University of science and technology.

Conflicts of Interest: The authors declare no conflict of interest.

Appendix A

Degree of grey incidence was calculated using Grey System theory (Equations (9) and (10)) (take *HE* for example):

Step 1: Dimensionless

Step 2: Discrepancy

Step 3: Extremum

$$\max_l \max_k |\bar{x}_0(k) - \bar{x}_l(k)| = 2.755 \text{ and } \min_l \min_k |\bar{x}_0(k) - \bar{x}_l(k)| = 0$$

Step 4: Closeness

Table A1. Dimensionless of Grey System theory for TPHS.

Items		Experiment_									
		1	2	3	4	5	6	7	8	9	10
<i>HE</i>	\bar{X}_0	1.000	0.995	1.039	1.110	0.947	1.046	1.057	1.065	1.057	0.864
	\bar{X}_1										
Feed concentration	\bar{X}_1	1.000	1.741	2.332	3.068	3.627	1.099	1.726	2.422	2.987	3.620
Feed pressure	\bar{X}_2	1.000	1.250	1.500	1.000	1.250	1.500	1.000	1.250	1.500	1.000
Aperture size	\bar{X}_3	1.000	1.200	1.400	1.000	1.200	1.400	1.000	1.200	1.400	1.000
Diameter of spigot	\bar{X}_4	1.000	1.333	1.000	1.333	1.000	1.333	1.000	1.333	1.000	1.333
Diameter of vortex finder	\bar{X}_5	1.000	1.333	1.667	2.000	1.000	1.333	1.667	2.000	1.000	1.333

Table A2. Discrepancy of Grey System theory for TPHS.

$ \overline{X}_l - \overline{X}_0 $		Experiment_									
		1	2	3	4	5	6	7	8	9	10
Feed concentration	$\overline{X}_l - \overline{X}_0$	0.000	0.746	1.294	1.957	2.680	0.054	0.669	1.357	1.930	2.755
Feed pressure	$\overline{X}_l - \overline{X}_0$	0.000	0.255	0.461	0.110	0.303	0.454	0.057	0.185	0.443	0.136
Aperture size	$\overline{X}_l - \overline{X}_0$	0.000	0.205	0.361	0.110	0.253	0.354	0.057	0.135	0.343	0.136
Diameter of spigot	$\overline{X}_l - \overline{X}_0$	0.000	0.338	0.039	0.223	0.053	0.288	0.057	0.268	0.057	0.469
Diameter of vortex finder	$\overline{X}_l - \overline{X}_0$	0.000	0.338	0.628	0.890	0.053	0.288	0.609	0.935	0.057	0.469

Table A3. Closeness of Grey System theory for TPHS.

$r(\overline{x}_0(k), \overline{x}_l(k))$		Experiment_										Average
		1	2	3	4	5	6	7	8	9	10	
Feed concentration	$r(\overline{x}_0(k), \overline{x}_1(k))$	1.000	0.649	0.516	0.413	0.339	0.962	0.673	0.504	0.417	0.333	0.581
Feed pressure	$r(\overline{x}_0(k), \overline{x}_2(k))$	1.000	0.844	0.749	0.926	0.820	0.752	0.960	0.882	0.757	0.910	0.860
Aperture size	$r(\overline{x}_0(k), \overline{x}_3(k))$	1.000	0.870	0.792	0.926	0.845	0.795	0.960	0.911	0.800	0.910	0.881
Diameter of spigot	$r(\overline{x}_0(k), \overline{x}_4(k))$	1.000	0.803	0.973	0.861	0.963	0.827	0.960	0.837	0.960	0.746	0.893
Diameter of vortex finder	$r(\overline{x}_0(k), \overline{x}_5(k))$	1.000	0.803	0.687	0.608	0.963	0.827	0.693	0.596	0.960	0.746	0.788

Appendix B

Prediction of performance evaluation for TPHS was estimated using GM(1,N) model (Equations (9) and (10)) based on the dimensionless sequence \bar{X}_0 and \bar{X}_I (see Table A1 in Appendix A) (take HE for example):

Step 1: Accumulated generation operation (AGO)

Table A4. Accumulated generation operation of \bar{X}_0 and \bar{X}_I

Items		Experiment									
		1	2	3	4	5	6	7	8	9	10
HE		1.000	1.995	3.034	4.144	5.091	6.136	7.194	8.259	9.316	10.285
d_{50c}	$\sum \bar{x}_0(k)$	1.000	2.087	3.109	4.174	5.413	6.413	7.457	8.543	9.630	10.761
I		1.000	2.028	3.065	4.003	4.834	5.863	6.935	7.909	8.829	9.817
Feed concentration	$\sum \bar{x}_1(k)$	1.000	2.741	5.074	8.142	11.769	12.868	14.594	17.016	20.003	23.622
Feed pressure	$\sum \bar{x}_2(k)$	1.000	2.250	3.750	4.750	6.000	7.500	8.500	9.750	11.250	12.250
Aperture size	$\sum \bar{x}_3(k)$	1.000	2.200	3.600	4.600	5.800	7.200	8.200	9.400	10.800	11.800
Diameter of spigot	$\sum \bar{x}_4(k)$	1.000	2.333	3.333	4.667	5.667	7.000	8.000	9.333	10.333	11.667
Diameter of vortex finder	$\sum \bar{x}_5(k)$	1.000	2.333	4.000	6.000	7.000	8.333	10.000	12.000	13.000	14.333

Step 2: Neighbor means sequence

Table A5. Mean generation of $\bar{x}_0(k)$.

Items		Experiment									
		1	2	3	4	5	6	7	8	9	10
HE	$z_0^{(1)}(k)$	1.498	2.514	3.589	4.617	5.613	6.665	7.726	8.787	9.800	1.498
d_{50c}	$\frac{\bar{x}_0^{(1)}(k) + \bar{x}_0^{(1)}(k-1)}{2}$	1.543	2.598	3.641	4.793	5.913	6.935	8.000	9.087	10.196	1.543
I		1.514	2.546	3.534	4.419	5.349	6.399	7.422	8.369	9.323	1.514

Step 3: Matrix **B** and **y**

$$\mathbf{B} = \begin{bmatrix} z_0^{(1)}(2)\bar{x}_1^{(1)}(2) \cdots \bar{x}_n^{(1)}(2) \\ \dots \\ z_0^{(1)}(m)\bar{x}_1^{(1)}(m) \cdots \bar{x}_n^{(1)}(m) \end{bmatrix} = \begin{bmatrix} 1.4982.7412.2502.2002.3332.333 \\ 2.5145.0743.7503.6003.3334.000 \\ 3.5898.1424.7504.6004.6676.000 \\ 4.61711.7696.0005.8005.6677.000 \\ 5.61312.8687.5007.2007.0008.333 \\ 6.66514.5948.5008.2008.00010.000 \\ 7.72617.0169.7509.4009.33312.000 \\ 8.78720.00311.25010.80010.33313.000 \\ 9.80023.62212.25011.80011.66714.333 \end{bmatrix}$$

$$\mathbf{y} = \begin{bmatrix} \bar{x}_1^{(1)}(2) \\ \vdots \\ \bar{x}_1^{(1)}(m) \end{bmatrix} = [0.995 \ 1.039 \ 1.110 \ 0.947 \ 1.046 \ 1.057 \ 1.065 \ 1.057 \ 0.970]^T$$

Step 4: Sequence of parameter \hat{a}

$$\hat{a} = [a, b_1, b_2, \dots, b_n] = (\mathbf{B}^T \mathbf{B})^{-1} \mathbf{B}^T \mathbf{y} = [1.842 \ -0.019 \ -6.227 \ 7.902 \ -0.001 \ 0.175]$$

Step 5: Prediction for the dimensionless HE

$$\text{For HE: } \bar{x}_0(k) = \frac{(-1.842\bar{x}_0^{(1)}(k-1) - 0.019\bar{x}_1^{(1)}(k) - 6.227\bar{x}_2^{(1)}(k) + 7.902\bar{x}_3^{(1)}(k) - 0.001\bar{x}_4^{(1)}(k) + 0.175\bar{x}_5^{(1)}(k)) / (1 + 1.842/2)}{1 + 1.842/2}$$

Similarly: Prediction for the dimensionless I and d_{50c}

$$\text{For } I: \bar{x}_0(k) = \frac{(-1.604\bar{x}_0^{(1)}(k-1) - 0.129\bar{x}_1^{(1)}(k) - 9.021\bar{x}_2^{(1)}(k) + 10.994\bar{x}_3^{(1)}(k) + 0.016\bar{x}_4^{(1)}(k) - 0.035\bar{x}_5^{(1)}(k))}{(1 + 1.604/2)}$$

$$\text{For } d_{50c}: \bar{x}_0(k) = \frac{(-1.690\bar{x}_0^{(1)}(k-1) + 0.065\bar{x}_1^{(1)}(k) - 9.541\bar{x}_2^{(1)}(k) + 11.632\bar{x}_3^{(1)}(k) - 0.127\bar{x}_4^{(1)}(k) - 0.142\bar{x}_5^{(1)}(k))}{(1 + 1.690/2)}$$

Step 6: Prediction model

$$\begin{bmatrix} \bar{x}_0(k)_{HE} \\ \bar{x}_0(k)_I \\ \bar{x}_0(k)_{d_{50c}} \end{bmatrix} = \begin{bmatrix} -0.959 & -0.010 & -3.242 & 4.113 & -0.0004 & 0.091 \\ -1.604 & -0.129 & -9.021 & 10.994 & 0.016 & -0.035 \\ -0.916 & -0.035 & -6.171 & 6.305 & -0.0687 & -0.077 \end{bmatrix} \begin{bmatrix} \bar{x}_0^{(1)}(k-1)_{HE} & \bar{x}_0^{(1)}(k-1)_I & \bar{x}_0^{(1)}(k-1)_{d_{50c}} \\ \bar{x}_1^{(1)}(k) & \bar{x}_1^{(1)}(k) & \bar{x}_1^{(1)}(k) \\ \bar{x}_2^{(1)}(k) & \bar{x}_2^{(1)}(k) & \bar{x}_2^{(1)}(k) \\ \bar{x}_3^{(1)}(k) & \bar{x}_3^{(1)}(k) & \bar{x}_3^{(1)}(k) \\ \bar{x}_4^{(1)}(k) & \bar{x}_4^{(1)}(k) & \bar{x}_4^{(1)}(k) \\ \bar{x}_5^{(1)}(k) & \bar{x}_5^{(1)}(k) & \bar{x}_5^{(1)}(k) \end{bmatrix}$$

Appendix C

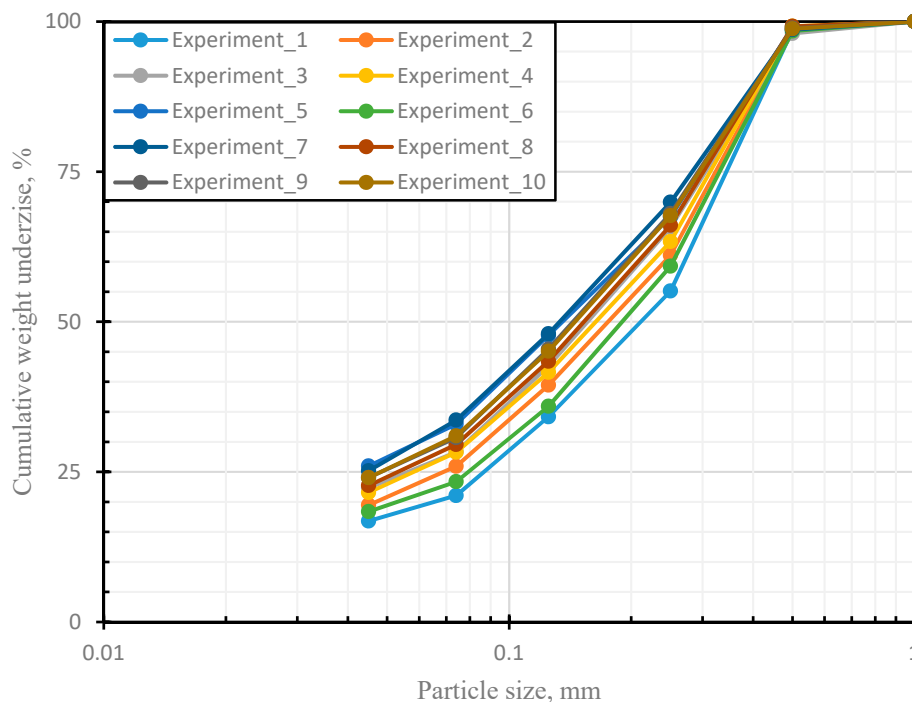


Figure A1. Size distribution of feed corresponding to each experiment for TPHS.

References

- Wasilewski, M. Analysis of the effects of temperature and the share of solid and gas phases on the process of separation in a cyclone suspension preheater. *Sep. Purif. Technol.* **2016**, *168*, 114–123. [[CrossRef](#)]
- Li, X.; Xu, H.; Liu, J.; Zhang, J.; Li, J.; Gui, Z. Cyclonic state micro-bubble flotation column in oil-in-water emulsion separation. *Sep. Purif. Technol.* **2016**, *165*, 101–106. [[CrossRef](#)]
- Chen, L.; You, Z.; Xie, H.; Zhang, H.; Li, Y.; Wei, Z. Fluidized hydrocyclone for continuous centrifugal concentration. *Sep. Purif. Technol.* **2017**, *52*, 1283–1288. [[CrossRef](#)]
- Bradley, D. *The Hydrocyclone: International Series of Monographs in Chemical Engineering*; Elsevier: Amsterdam, The Netherlands, 2013; Volume 4.

5. Wang, G.; Liu, Q.; Wang, C.; Dong, L.; Processes, L.S.J. Study of blockage diagnosis for hydrocyclone using vibration-based technique based on wavelet denoising and discrete-time fourier transform method. *Processes* **2020**, *8*, 440. [[CrossRef](#)]
6. Chu, L.-Y.; Yu, W.; Wang, G.-J.; Zhou, X.-T.; Chen, W.-M.; Dai, G.-Q. Enhancement of hydrocyclone separation performance by eliminating the air core. *Chem. Eng. Process. Process Intensif.* **2004**, *43*, 1441–1448. [[CrossRef](#)]
7. Dueck, J.; Farghaly, M.; Neesse, T. The theoretical partition curve of the hydrocyclone. *Miner. Eng.* **2014**, *62*, 25–30. [[CrossRef](#)]
8. Santana, R.C.; Farnese, A.C.; Fortes, M.C.; Ataíde, C.H.; Barrozo, M.A. Influence of particle size and reagent dosage on the performance of apatite flotation. *Sep. Purif. Technol.* **2008**, *64*, 8–15. [[CrossRef](#)]
9. Vieira, L.G.M.; Barrozo, M.A.S. Effect of vortex finder diameter on the performance of a novel hydrocyclone separator. *Miner. Eng.* **2014**, *57*, 50–56. [[CrossRef](#)]
10. Vieira, L.G.; Silva, D.O.; Barrozo, M.A. Effect of inlet diameter on the performance of a filtering hydrocyclone separator. *Chem. Eng. Technol.* **2016**, *39*, 1406–1412. [[CrossRef](#)]
11. Silva, N.K.G.; Silva, D.O.; Vieira, L.G.M.; Barrozo, M.A.S. Effects of underflow diameter and vortex finder length on the performance of a newly designed filtering hydrocyclone. *Powder Technol.* **2015**, *286*, 305–310. [[CrossRef](#)]
12. Obeng, D.; Morrell, S.; Napier-Munn, T. Application of central composite rotatable design to modelling the effect of some operating variables on the performance of the three-product cyclone. *Int. J. Miner. Process.* **2005**, *76*, 181–192. [[CrossRef](#)]
13. Nenu, R.K.T.; Yoshida, H. Comparison of separation performance between single and two inlets hydrocyclones. *Adv. Powder Technol.* **2009**, *20*, 195–202. [[CrossRef](#)]
14. Hwang, K.-J.; Hwang, Y.-W.; Yoshida, H. Design of novel hydrocyclone for improving fine particle separation using computational fluid dynamics. *Chem. Eng. Sci.* **2013**, *85*, 62–68. [[CrossRef](#)]
15. Chu, L.Y.; Chen, W.M.; Lee, X.Z. Effect of structural modification on hydrocyclone performance. *Sep. Purif. Technol.* **2000**, *21*, 71–86. [[CrossRef](#)]
16. Delgadillo, J.A.; Rajamani, R.K. Exploration of hydrocyclone designs using computational fluid dynamics. *Int. J. Miner. Process.* **2007**, *84*, 252–261. [[CrossRef](#)]
17. Silva, D.; Facanha, J.; Vieira, L.; Barrozo, M.A. Experimental Study of the Influence of Vortex Finder Geometry on Hydrocyclones Performance. *Mater. Sci. Forum* **2012**, *727–728*, 1848–1853. [[CrossRef](#)]
18. Wang, C.; Chen, J.; Shen, L.; Hoque, M.M.; Ge, L.; Evans, G.M. Inclusion of screening to remove fish-hook effect in the three products hydro-cyclone screen (TPHS). *Miner. Eng.* **2018**, *122*, 156–164. [[CrossRef](#)]
19. Jianzhong, C.; Lijuan, S.; Chuazhen, W. Desliming performance of the three-product cyclone classification screen. *J. China Univ. Min. Technol.* **2016**, *45*, 807–813.
20. Wang, C.; Chen, J.; Shen, L.; Ge, L. Study of flow behaviour in a three products hydrocyclone screen: Numerical simulation and experimental validation. *Physicochem. Probl. Miner. Process.* **2019**, *55*, 879–895. [[CrossRef](#)]
21. Wills, B.A.; Napier-Munn, T. *Wills' Mineral Processing Technology: An Introduction to the Practical Aspects of Ore Treatment and Mineral Recovery*; Butterworth-Heinemann: Oxford, UK, 2015.
22. Julong, D. Control problems of grey systems. *Sys. Contr. Lett.* **1982**, *1*, 288–294. [[CrossRef](#)]
23. Liu, S.; Forrest, J.Y.L. *Grey Systems: Theory and Applications*; Springer: Berlin/Heidelberg, Germany, 2010.
24. Julong, D. Introduction to grey system theory. *J. Grey Syst.* **1989**, *1*, 1–24.
25. Jiang, P.; Wang, W.; Hu, Y.-C.; Chiu, Y.-J.; Tsao, S.-J. Pattern classification using tolerance rough sets based on non-additive grey relational analysis and DEMATEL. *Grey Syst. Theory Appl.* **2020**, *10*, 1108–1125. [[CrossRef](#)]
26. Rawat, M.; Lad, B.K.; Sharma, A. Simulation-based joint optimization of fleet system modularity and level of repair decisions considering different failure rates of components. *Grey Syst. Theory Appl.* **2020**, *10*, 377–390. [[CrossRef](#)]
27. Wei, S.; Lijuan, S.; Jianzhong, C.; Shangjie, S. Application of grey correlation to key factor analysis for separation effects of dense-medium cyclones. *Min. Process. Equipmen* **2013**, *41*, 6.
28. China, S.A.O.T.P.S.R.O. *GB/T477-2008 Method for Size Analysis of Coal*; Standards Press of China: Beijing, China, 2009.
29. Peng, F.; Chang, D. Solving mass balance problems in coal processing using the constrained/weighted least-squares method. *Fuel Energy Abstr.* **1996**, *17*, 384–385. [[CrossRef](#)]
30. Kelsall, D. A further study of the hydraulic cyclone. *Chem. Eng. Sci.* **1953**, *2*, 254–272. [[CrossRef](#)]

31. Frachon, M.; Cilliers, J. A general model for hydrocyclone partition curves. *Chem. Eng. J.* **1999**, *73*, 53–59. [[CrossRef](#)]
32. Barsky, E.; Barsky, M. Relationship between fractional separation curves and quantitative optimization criteria in the separation of pourable materials. *Phys. Sep. Sci. Eng.* **2004**, *13*, 41–51. [[CrossRef](#)]
33. Randić, D. Proposition of new indices and parameters for grain size classification efficiency estimation. *J. Min. Metall. A Min.* **2008**, *44*, 17–23.
34. Honaker, R.; Boaten, F.; Luttrell, G. Ultrafine coal classification using 150mm gMax cyclone circuits. *Miner. Eng.* **2007**, *20*, 1218–1226. [[CrossRef](#)]



© 2020 by the authors. Licensee MDPI, Basel, Switzerland. This article is an open access article distributed under the terms and conditions of the Creative Commons Attribution (CC BY) license (<http://creativecommons.org/licenses/by/4.0/>).